10-4-2022

The formation of monosubstituted cyclopropenylidene derivatives in the interstellar medium via neutral-neutral reaction pathways

Athena R. Flint
University of Mississippi

Ryan C. Fortenberry
University of Mississippi

Recommended Citation

Flint, A., & Fortenberry, R. (2022). The Formation of Monosubstituted Cyclopropenylidene Derivatives in the Interstellar Medium via Neutral–Neutral Reaction Pathways. The Astrophysical Journal, 938(1), 15. doi: 10.3847/1538-4357/ac8f4a

The Astrophysical Journal, 938:15 (11pp), 2022 October 10 https://doi.org/10.3847/1538-4357/ac8f4a

The Formation of Monosubstituted Cyclopropenylidene Derivatives in the Interstellar Medium via Neutral–Neutral Reaction Pathways

Athena R. Flint and Ryan C. Fortenberry
Department of Chemistry and Biochemistry, University of Mississippi University, Mississippi 38677-1848, USA; r410@olemiss.edu
Received 2022 July 26; revised 2022 August 29; accepted 2022 September 3; published 2022 October 11

Abstract

Five substituted cyclopropenylidene derivatives (c-C_3HX, X=CN, OH, F, NH_2), all currently undetected in the interstellar medium (ISM), are found herein to have mechanistically viable, gas-phase formation pathways through neutral–neutral additions of ·X onto c-C_3H_2. The detection and predicted formation mechanism of c-C_3HC_2H introduces a need for the chemistry of c-C_3H_2 and any possible derivatives to be more fully explored. Chemically accurate CCSD(T)-F12/cc-pVTZ-F12 calculations provide exothermicities of additions of various radical species to c-C_3H_2, alongside energies of submerged intermediates that are crossed to result in product formation. Of the novel reaction mechanisms proposed, the addition of the cyano radical is the most exothermic at -16.10 kcal mol^{-1}. All five products are found to or are expected to have at least one means of associating barrierlessly to form a submerged intermediate, a requirement for the cold chemistry of the ISM. The energetically allowed additions arise as a result of the strong electrophilicity of the radical species as well as the product stability gained through substituent-ring conjugation.

Unified Astronomy Thesaurus concepts: Astrochemistry (75); Interdisciplinary astronomy (804); Neutral-neutral reactions (2265); Quantum-chemical calculations (2232)

1. Introduction

The recent discovery of ethynyl cyclopropenylidene (c-C_3HC_2H) in the interstellar medium (ISM; Cernicharo et al. 2021) marks the first-time detection of a functionalized cyclopropenylidene (c-C_3H_2) derivative in an astrophysical environment. The plausibility of an ethynyl-functionalized c-C_3H_2 derivative was first hypothesized by Vrtilek et al. (1987) and computationally validated by Cooper & Murphy (1988) before being detected in the laboratory by Travers et al. (1997). The structural isomers of c-C_3HC_2H have also been studied in detail, showing that this form is the lowest in energy for the singlet spin multiplicity (Seburg et al. 1997; Karton & Thimmakondu 2022). Following the astrophysical detection of c-C_3HC_2H (Cernicharo et al. 2021), a mechanistic study of its formation found that c-C_3HC_2H may form through a gas-phase reaction between c-C_3H_2 and the ethynyl radical (Fortenberry 2021). These results open a veritable Pandora's box for further astrochemical analysis regarding the formation of c-C_3H_2 and its family of derivatives (He et al. 2022; Yang et al. 2021).

For astrochemists, c-C_3H_2 is an incredibly convenient source for cosmic chemical reactions; c-C_3H_2 and its derivatives likely have a significant abundance throughout the cosmos, as c-C_3H_2 is one of the most abundant molecules in the universe. Spectroscopic detection of c-C_3H_2 occurs readily in a variety of astronomical sources ranging from circumstellar envelopes to gas clouds and even to planetary atmospheres (Thaddeus et al. 1981; Matthews & Irvine 1985; Thaddeus et al. 1985; Seaquist & Bell 1986; Cox et al. 1987; Vrtilek et al. 1987; Madden et al. 1989; Lucas & Liszt 2000; Oike et al. 2004; Teyssier et al. 2004; Qi et al. 2013; Nixon et al. 2020). The detections of this molecule even include the ^{2}D (Bell et al. 1986; Majumdar et al. 2017) and ^{13}C (Gomez Gonzalez et al. 1986; Madden et al. 1986; Spezzano et al. 2013) isotopologues, implying that molecular abundances are notable enough for such isotopic substitution to be observable. For example, the column density for c-C_3H_2 in the Magellanic Clouds is reported to be within 10 orders of magnitude of that of H_2 and 5 orders of magnitude of that of CO, putting its concentration on par with other abundant interstellar molecules such as CH_3OH (Heikkilä et al. 1999). The large dipole moment of 3.32 D for c-C_3H_2 as reported by Brown et al. (1987), resulting from its carbenic structure, makes it and its derivatives ripe for study and detection via rotational spectroscopy (Spezzano et al. 2012). The high interstellar concentrations of c-C_3H_2 make it a strong candidate for one of the chemical building blocks that form larger organic species (Tan et al. 2014). The potential of c-C_3H_2 is only increased by its unique chemical reactivity. The carbenic carbon, as with all carbenes, can accept or donate electron density through its empty p orbital or its lone pair, respectively. The π electrons can also be donated, while the orbitals they occupy can accept additional density. The astrochemical potential of this molecule, now corroborated by Cernicharo et al. (2021) and Fortenberry (2021) necessitates additional investigation into its chemistry especially for reactions with other, abundant molecules beyond ·C_2H.

The chemical diversity of the ISM may hold the key to unlocking the secrets that c-C_3H_2 and c-C_3HC_2H possess. In the ISM, the dominant gas-phase chemical species are closed- and open-shell charge-neutral molecules (Kaiser 2002; Smith 2011; McGuire 2021). The detection of c-C_3HC_2H in TMC-1 positions this species in the same environments in which c-C_3H_2 is known to exist in significant column densities. Given the coexistence of small monoradical species and c-C_3H_2 in the ISM, the formation of other monosubstituted cyclopropenylidene derivatives may take place through a mechanism similar to that proposed for c-C_3HC_2H (Fortenberry 2021). In this mechanism, barrierless

association of an ethynyl radical with the π density of c-C_3H_2 results in an intermediate with a disrupted aromaticity. Addition at the carbenic site of c-C_3H_2 results in a deeper-welled intermediate in which the ethynyl substituent is forced out of the plane of the molecule through Jahn–Teller distortions (Hoffmann et al. 1984; Chipman & Miller 1984). Movement between the two intermediates is possible through the migration of a hydrogen atom. Hydrogen release in the final step of the mechanism restores aromaticity to the molecule. Although interactions between c-C_3H_2 and small radicals will result in differing intermediate structures and reaction energetics, the variety and density of radical species in the ISM increases the likelihood of other similar reactions.

In particular, the ISM harbors the best physical conditions for c-C_3H_2 chemistry to occur. The relatively high reaction rates in the cold ISM for radical–neutral reactions, owing to the inverse dependence of temperature on rates for this reaction class (Smith 2011) show that the facile addition of $\cdot C_2H$ onto c-C_3H_2 follows a rule rather than creates an exception, motivating further study of these reactions. Cernicharo et al. (2021) state that the formation of c-C_3HCN, for which rotational (McCarthy et al. 1999) and vibrational (Westbrook et al. 2021) spectroscopic data exist but no astrophysical detection has yet occurred, likely follows a nearly identical pathway to that of c-C_3HC_2H (Cernicharo et al. 2021). This present work sets out to examine the reactivity of several monoradical species with c-C_3H_2. Below, pathways are established for reactions that are determined to be possible within the ISM providing candidates for spectroscopic detection as well as giving additional insight into the chemistry that drives interstellar processes.

2. Computational Methods

The chemical complexity of the molecules in this study necessitates the use of highly accurate quantum chemical treatments of their energies and structures but without the incursion of a large time penalty and computational cost. The primary level of theory used in this study, CCSD(T)-F12b/cc-pVTZ-F12 hereafter referred to as F12-TZ (Adler et al. 2007; Peterson et al. 2008; Knizia et al. 2009; Hill & Peterson 2010), applies explicit correlation to the triple-zeta correlation-consistent polarized valence basis sets (Dunning 1989; Kendall et al. 1992; Woon & Dunning 1993) and the current "gold standard" CCSD(T) method (Raghavachari et al. 1989; Hampel et al. 1992; Knowles et al. 1993; Deegan & Knowles 1994). CCSD(T), read as coupled cluster singles, doubles, and perturbative triples, uses the electronic excitation operator to represent electron correlation in the construction of the wave function. The F12 modification introduces additional terms that better describe the short-range interactions between electrons within the overall electron correlation (Knizia et al. 2009). Application of explicit correlation to CCSD(T)/cc-pVTZ decreases computation time and increases chemical accuracy relative to its larger basis set counterpart (Gyorffy & Werner 2018).

Minima on reaction pathways are geometrically optimized with F12-TZ using the MOLPRO quantum chemical software (Werner et al. 2012, 2020a, 2020b) as are the harmonic vibrational frequencies. Dipole moments are calculated using these methods for products of reaction only. All energies reported are the result of adding the electronic energy for the optimized structure and the zero-point vibrational energy. Transition states are optimized with Møller–Plesset second-order perturbation theory (MP2; Møller & Plesset 1934; Amos et al. 1991; Knowles et al. 1991) and an aug-cc-pVTZ basis set using the GAUSSIAN16 quantum chemical program (Frisch et al. 2019). The single-point energy of this optimized reference geometry is calculated at the F12-TZ level in MOLPRO in order to be consistent in the determination of the reaction energies (Ramal-Olmedo et al. 2021).

2.1. Potential Energy Scans

Relaxed potential energy scans are generated to link reactants to intermediates and intermediates to products along a predefined reaction coordinate. This type of scan takes a set of points, created by fixing a single geometric variable at certain values, and optimizes the remaining geometric variables to obtain the electronic energy as a function of the fixed variable. The points within these scans are generated by varying the coordinate of interest, corresponding to the distance between the associating or dissociating groups, over a 1–5 Å distance with a 0.1 Å step size. In order to lessen the computational cost, all points within the ground-state relaxed potential energy scans are optimized with MP2/aug-cc-pVTZ, and a subsequent single-point energy is calculated at the F12-TZ level of theory using MOLPRO. The introduction of diffuse functions during the optimization portion of the calculations allows for the inclusion of long-range interactions in the behavior of the system, which are vital for chemically accurate representations of distantly interacting species.

There are occasions where points within the relaxed potential energy scans exhibit multireference effects. These arise when a system is not well defined by the use of single-reference electron correlation procedures, which can be indicated by the T1 diagnostic in a coupled cluster calculation (Lee & Taylor 1989). In these cases, the effects of electronic excitations on the geometries along the reaction coordinate must be considered. Restricted potential energy scans are done with inclusion of the first four electronically excited states of a complex during associations or dissociations where multireference behavior is seen. These restricted scans, in contrast to a relaxed scan, do not allow any variables to change other than the displacement between the two groups, which drastically reduces computation time. All points within the excited-state restricted potential energy scans are evaluated in PSI4 (Turney et al. 2012; Parrish et al. 2017) by calculating single-point energies of the F12-TZ-optimized geometry using an equation-of-motion (EOM-CCSD; Stanton & Bartlett 1993; Krylov 2008) method and the aug-cc-pVTZ basis set. Points are generated that correspond to the same variable and step size as their ground-state counterparts. Electronically excited restricted scans can reveal intersections between different electronic states on the potential surface due to the variance of a single coordinate to produce them (Yarkony 2001; Domcke & Yarkony 2012; Schuurman & Stolow 2018).

The analysis of an excited-state restricted potential energy scan may require a knowledge of the molecular orbitals (MOs) of the complex. When necessary, these are calculated in GAUSSIAN16 with ROHF/aug-cc-pVTZ and visualized with Gabedit (Allouche 2010, 2017). The contributions of various excitations to an electronically excited state as calculated by PSI4 can be modeled using these MOs. MO analyses can also be used to examine electron delocalization and electron density in the starting materials and products of the reaction in order to determine stability and reactivity.

2.2. Chemical Reactions in the ISM

Due to the low photon flux in the areas of the ISM where radical–neutral, gas-phase reactions are common, there exist energetic restrictions on the pathways these reactions follow. The gas-phase reaction between two species in a such a low-temperature environment with no nearby photon source must require no additional energy input to proceed, as there is no energy source to access outside of the energy inherent to the molecules (Puzzarini 2022). As a consequence, the reactants must be an energy maximum on their respective reaction coordinate. Therefore, the hypothesized reaction must satisfy certain conditions in order to be plausible within the confines of the interstellar medium. For bimolecular reactions that form a single intermediate such as those proposed here, the association of the two reactants must be barrierless (Puzzarini 2022; Grosselin & Fortenberry 2022). Furthermore, the overall reaction must not be endothermic. Creating products of such a reaction would require the system to gain some amount of energy from an outside source.

For an exothermic pathway, there will be excess energy within the system due to the lowering of the overall energy of the chemical species on the pathway. This is most easily dissipated in the form of kinetic energy by a dissociation of a leaving group in the final step of the reaction (Puzzarini 2022). For the reactions studied herein, a hydrogen radical serves this purpose:

$$c - C_3H_2 + \cdot X \rightarrow c - C_3HX + \cdot H. \quad (1)$$

Without this translational energy sink, the large amount of excess energy would need to be lost by radiative processes (Puzzarini 2022), which are assumed to be unable to occur within this class of molecules without destruction of the desired product.

The ability of a reaction pathway to proceed is also impacted by the energies of the intermediates and transition states created along the pathway. As the reaction proceeds, the procession across submerged transition states affects the feasibility of a given reaction (Puzzarini 2022). Additionally, the expenditure of larger amounts of energy from the reserve created by the initial association in order to leave a submerged well may impact product abundances and the intermediates on a multistep pathway from which products are able to form. The dissociation of an intermediate on a pathway into the desired products can be encouraged if the intermediate is less submerged. Of the chemical processes in the ISM, dissociation can compete with radiative association. The rate at which radiative association occurs is increased by, among other factors, the energetic depth of the submerged well. In cases where these two processes could feasibly compete, if the dissociation lacks an exit barrier, radiative association becomes too slow in comparison. It follows that in cases where a leaving group may struggle to dissociate from an intermediate, raising the energy of that intermediate will discourage radiative association and therefore promote the success of the reaction (Herbst 2001, 2021).

3. Results and Discussion

Table 1 lists 13 radical species and the energetics of their additions to c-C_3H_2. The structures of the 17 resulting substituted cyclopropenylidenes are provided in Figure 1, with their names and chemical formulae following in Table 2; ΔE_{rxn} is defined as the difference between the zero-point-corrected electronic energies for the products and reactants of the pathway as a whole. Of the hypothetical reaction pathways studied, 12 of the 17 products, resulting from the addition of nine different radicals, result from overall endothermic mechanisms, and are not possible in regions of space without a significant energy source or activating surface. The most exothermic of these additions, that of $\cdot C_2H$, produces the only substituted cyclopropenylidene derivative detected in the ISM thus far. These results present five additional candidates with net-exothermic pathways for spectroscopic detection: c-C_3HCN, c-C_3HF, ap-c-C_3HOH, sp-c-C_3HOH, and c-C_3HNH_2. The cyano (McKellar 1940; Adams 1941; Jefferts et al. 1970; Henkel et al. 1988), fluorine (Suess & Urey 1956; Cameron 1973; Jr & York 1981), hydroxy (Weinreb et al. 1963; Heiles 1968; Dickey et al. 1981; Crutcher et al. 1981; Storey et al. 1981), and amino (van Dishoeck et al. 1993; Melosso et al. 2020) radicals exist, although in varying concentrations, in interstellar space, underpinning the detectability of the products of reactions involving them.

Table 1
ΔE_{rxn} for c-C_3H_2 and $\cdot X$ and the Dipole Moments of the Resulting Products

$\cdot X$	ΔE_{rxn} (kcal mol^{-1})	Dipole Moment (D)
$\cdot C_2H$	−26.77	3.58
$\cdot CN$	−16.10	3.06
$\cdot F$	−10.77	2.99
ap-$\cdot OH$	−4.73	2.36
$\cdot NH_2$	−3.51	4.73
sp-$\cdot OH$	−2.56	4.83
ap-$\cdot OCH_3$	3.09	2.63
$\cdot NCO$	4.02	2.77
$\cdot CH_3$	4.68	3.76
sp-$\cdot OCH_3$	4.87	5.23
$\cdot SiH_3$	9.65	3.36
$\cdot CH_2OH$	9.67	3.55
$\cdot Cl$	15.31	3.06
ap-$\cdot SH$	16.02	2.76
sp-$\cdot SH$	17.08	4.16
$\cdot CHO$	18.62	3.30
$\cdot PH_2$	23.57	3.44
$\cdot OCN$	37.15	4.92

Note. The result for the energy of the $\cdot C_2H$ addition arises from the same structure reported by Fortenberry (2021). Antiperiplanar (ap) and synperiplanar (sp) designations are given to rotameric pairs, and describe a 0° or 180° dihedral angle, respectively, between the carbenic carbon and the in-plane hydrogen of the substituent.

3.1. Formation of c-C3HCN

Figure 2 displays the reaction pathway of the addition of $\cdot CN$ to c-C_3H_2 to form c-C_3HCN. As predicted by Cernicharo et al. (2021), the pathway for the cyano addition is similar to the formation mechanism for c-C_3HC_2H. The data compiled in Table 3 compare the reaction energies for the addition of both radicals as well as the differences in energy between the formed products and both intermediates along the pathway. The addition of $\cdot C_2H$ is more exothermic by 11.1 kcal mol^{-1}, a substantial amount considering the low-energy environments in which these molecules form. Additionally, the energy differences between intermediates on the pathway and the products forming from them are smaller for the c-C_3HC_2H pathway. Comparatively, substitution with $\cdot C_2H$ requires that a smaller

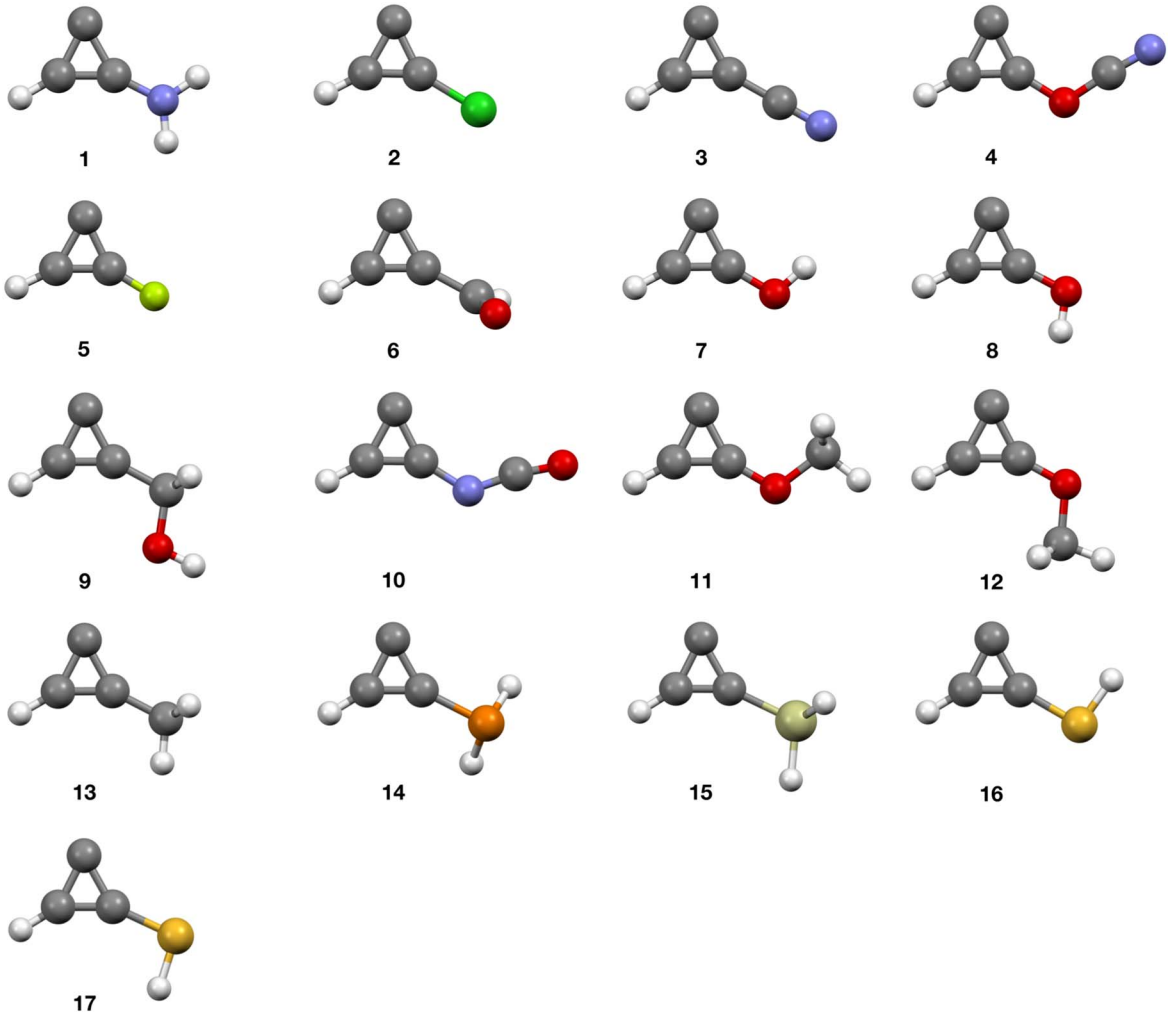

Figure 1. Products of cyclopropenylidene hydrogen-substitution with various radicals. Energetics of reaction are listed in Table 1. Table 2 lists their names and chemical formulae.

Table 2
Molecules Depicted in Figure 1

Figure Number	Molecule Name	Molecular Formula
1	Amino cyclopropenylidene	*c*-C_3HNH_2
2	Chloro cyclopropenylidene	*c*-C_3HCl
3	Cyano cyclopropenylidene	*c*-C_3HCN
4	Cyanate cyclopropenylidene	*c*-C_3HOCN
5	Fluoro cyclopropenylidene	*c*-C_3HF
6	Formyl cyclopropenylidene	*c*-C_3HCHO
7	*ap*-Hydroxyl cyclopropenylidene	*ap*-*c*-C_3HOH
8	*sp*-Hydroxyl cyclopropenylidene	*sp*-*c*-C_3HOH
9	Hydroxymethyl cyclopropenylidene	*c*-C_3HCH_2OH
10	Isocyanate cyclopropenylidene	*c*-C_3HNCO
11	*ap*-Methoxy cyclopropenylidene	*ap*-*c*-C_3HOCH_3
12	*sp*-Methoxy cyclopropenylidene	*sp*-*c*-C_3HOCH_3
13	Methyl cyclopropenylidene	*c*-C_3HCH_3
14	Phosphino cyclopropenylidene	*c*-C_3HPH_2
15	Silyl cyclopropenylidene	*c*-C_3HSiH_3
16	*ap*-Sulfanyl cyclopropenylidene	*ap*-*c*-C_3HSH
17	*sp*-Sulfanyl cyclopropenylidene	*sp*-*c*-C_3HSH

amount of the energy reserve created by formation of a submerged intermediate is lost upon dissociation of a hydrogen atom; see Table 4; *c*-C_3HCN remains undetected anywhere in space at the time of writing, which demonstrates a need for a deeper exploration into the formation and dissociation rates of the intermediates along this pathway.

3.2. Formation of *c*-C_3HOH

Figure 3 shows the reaction pathway for the addition of ·OH to *c*-C_3H_2, forming *c*-C_3HOH. Several aspects of this formation distinguish it from other additions of this type. Most notably, this addition results in two distinct products that are minima on their respective potential surfaces, which are separated by a rotation barrier. The transition state that represents the maximum of this rotation barrier along the H-O-C coordinate is energetically inaccessible through the *c*-C_3H_2/·OH association pathway. Consequently, isomerization between the two once the product forms is not possible without outside energetic intervention.

This addition also creates a newly-accessible enantiomeric intermediate not found in the *c*-C_3HC_2H formation pathway. The association of ·OH with the lone-pair-bearing carbon of *c*-C_3H_2 results in the formation of these energetically distinct structures. Intermediate I2a in Figure 3 resembles the global-minimum intermediates of the *c*-C_3HC_2H and *c*-C_3HCN formation pathways. The key difference is the loss of C_s symmetry due to the location of the substituent hydrogen atom.

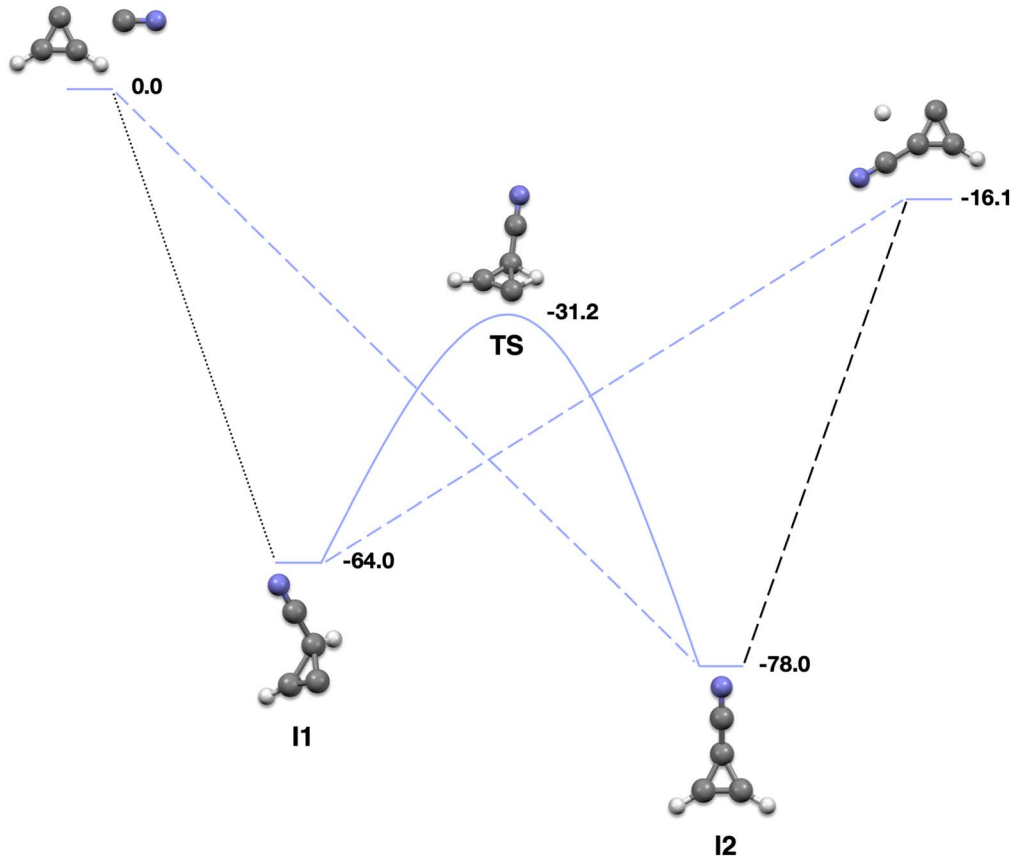

Figure 2. Reaction mechanism for the addition of ·CN onto *c*-C_3H_2. Highlighted connections indicate the most energetically likely formation route.

Table 3
Reaction Energies and Exit Energies for Energetically Allowed Radical Associations to *c*-C_3H_2

·*X*	ΔE_{rxn}	ΔE_{exit}, I1	ΔE_{exit}, I2a	ΔE_{exit}, I2b
·C_2H	−26.77	43.59	57.02	
·CN	−16.10	47.93	61.90	
ap-·OH	−4.73	43.28	46.55	48.68
sp-·OH	−2.56		48.73	50.20
·F	−10.77	52.36	56.54	51.74
·NH_2	−3.51	35.79	40.69	47.11

Note. Values for ·C_2H originate from structures identical to those presented by Fortenberry (2021). All energies reported in kcal mol^{-1}.

Table 4
Intermediate and Transition State Energies Relative to Starting Materials for Allowed Associations onto *c*-C_3H_2

·*X*	E_{rel}, I1	E_{rel}, TSa	E_{rel}, TSb	E_{rel}, I2a	E_{rel}, I2b
·CN	−64.04	−31.25		−78.01	
ap-·OH	−48.01	−16.25	10.03	−51.28	−53.41
sp-·OH		−16.25		−51.28	−52.87
·F	−63.13	−26.90	0.72	−67.31	−62.52
·NH_2	−39.30	−11.81		−44.20	−50.62

Note. All energies reported in kcal mol^{-1}.

Figure 4 shows the stabilization in the singly-occupied molecular orbital (SOMO) and SOMO-1 of intermediate I2a as a result of the loss of symmetry and subsequent increase in interaction between the oxygen electron density and the partially filled orbital of the attached carbon. Intermediate I2b allows the entire hydroxyl group (·OH) to enter the plane of the ring forcing a carbon-bound hydrogen atom out of the plane. The out-of-plane hydrogen atom in this intermediate is found to be especially acidic resulting in the only dissociation in Figure 3 that is found to have no discernible exit barrier or to exhibit no significant multireference interference in the F12-TZ potential energy scan.

The possibilities for reactivity between ·OH and *c*-C_3H_2 expand further with the ability of ·OH to add barrierlessly to form any of the three types of intermediates in Figure 3. Intermediates I1 and I2a are able to interconvert via the transition state TSa. However, intermediate I2b cannot be accessed through hydroxy or hydrogen migration from intermediate I1 through transition state TSb due to energy restrictions as the transition state energy is greater than that of the reactants. Therefore, intermediate I2b may only be formed by direct association, while the other two intermediates may be formed by direct association or substituent migration. Interestingly, the enantiomers of intermediate I2b are able to interconvert through a relatively low but still overall submerged transition barrier TS_{I2b}. Although an association to form intermediate I2b would lock the molecule into that conformation type, the transition state present between the enantiomers does not allow this association to completely dictate product formation. Given that the difference between intermediates I2a and the two enantiomers of intermediate I2b is a single out-of-plane moiety, other, less significant transition states may exist that are similar to TS_{I2b} and allow alternative but similar migrations.

Although any of the three intermediates may form by ·OH association onto *c*-C_3H_2, the intermediates themselves are restricted into which product(s) they are able to form. All

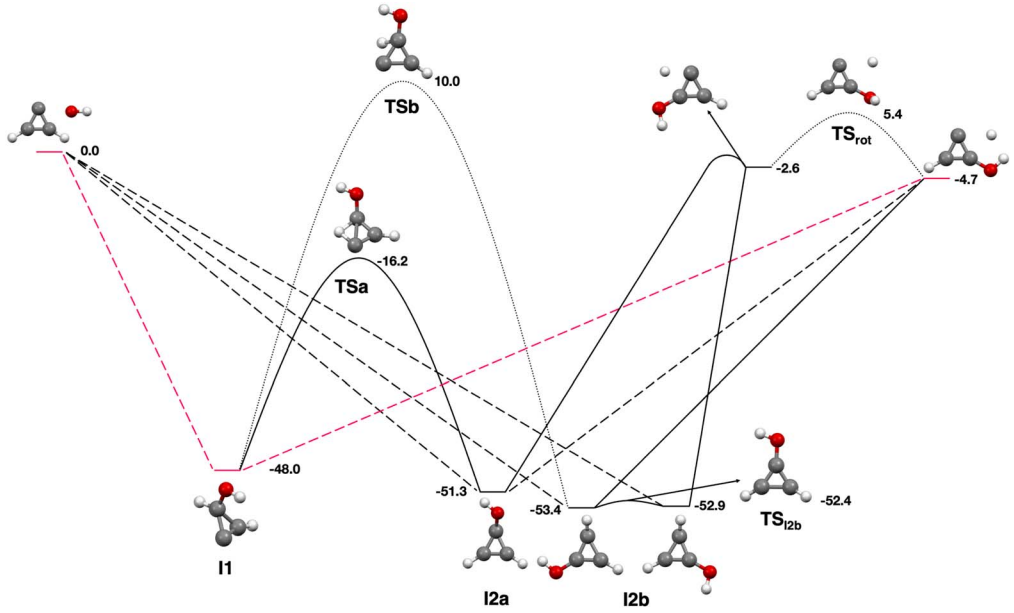

Figure 3. Reaction mechanism for the addition of ·OH onto *c*-C_3H_2. Highlighted connections indicate the most energetically likely formation route.

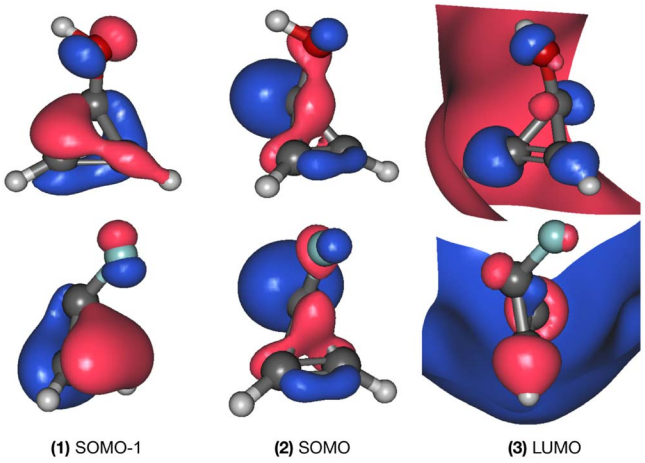

Figure 4. Frontier MOs of intermediate I2a for the formation of *c*-C_3HOH and *c*-C_3HF.

intermediates in Figure 3 have the possibility of forming at least one of the *c*-C_3HOH rotamers through hydrogen release. However, the intermediate formed by the initial association may force formation of a single product. Intermediate I1 is one such case. The structure of I1 is such that the HOCH dihedral angle about the substituent-bearing carbon approaches 180°, allowing H–Oσ density to donate into an MO with C–Hσ^* character, and vice versa. Additionally, some overlap is possible between the valence electron density of the oxygen and the nearby C−Cσ^* MOs. These effects propagate in the elongation of the C–C bond between the hydrogen-bearing carbons since the OH group is aligned to allow for stronger donation into an MO with a strong σ^* character. These stabilizing interactions result in a structure where the rotation of the COH bond to form the antiperiplanar product from I1 is much less than that for the alternative synperiplanar product. Therefore, release of a hydrogen from this intermediate only allows a single rotamer, *ap*-*c*-C_3HOH, to form. Intermediate I2a, accessible from I1 through TSa, leads to formation of either rotamer through hydrogen release. However, access to *sp*-*c*-C_3HOH is blocked through an exit barrier, shown by EOM-CCSD to be approximately 1 kcal in height, which cannot be traversed through an electronic excitation; *ap*-*c*-C_3HOH forms from this intermediate without such interference. Intermediate I2b is likely restricted to formation of *ap*-*c*-C_3HOH due to increased reaction rates. As a result, association to form I1 or I2a will result almost entirely in formation of the lower-energy rotamer.

The dipole moments for the two rotamers of *c*-C_3HOH are listed in Table 1. Of the products able to form through radical addition, the synperiplanar (*sp*-*c*-C_3HOH) product has the greatest dipole moment, while the antiperiplanar (*ap*-*c*-C_3HOH) product has the smallest. Even though this means that *sp*-*c*-C_3HOH is readily detectable via rotational spectroscopy, the formation of this rotamer results in less energetic stabilization for the pathway as a whole. Additionally, this product can only form from hydrogen release from I2b. Therefore, *sp*-*c*-C_3HOH can only form if direct association to form I2b forms the necessary enantiomer, or if migration across TS_{I2b} upon formation of the other enantiomer is faster than hydrogen release from that structure; *ap*-*c*-C_3HOH has the ability to form through hydrogen dissociation from any intermediate. Given the greater number of routes to formation of this product compared to *sp*-*c*-C_3HOH, which includes the dominant route (highlighted in Figure 3) of product formation, *ap*-*c*-C_3HOH is likely the major product of this reaction pathway. Higher relative interstellar abundances will likely be observed for *ap*-*c*-C_3HOH if detected. However, the intensity of the rotational spectrum that *ap*-*c*-C_3HOH produces is reduced by its much weaker dipole moment in comparison to that of *sp*-*c*-C_3HOH.

The formation of *ap*-*c*-C_3HOH (Figure 3), compared to the formation of *c*-C_3HC_2H, is much less energetically favorable if considering the pathway as a whole. However, the decrease in energy expenditure from the submerged well for the release of a hydrogen atom from I1 for the antiperiplanar conformation of *c*-C_3HOH may influence comparative formation abilities and reaction rates making it worth further kinetic study.

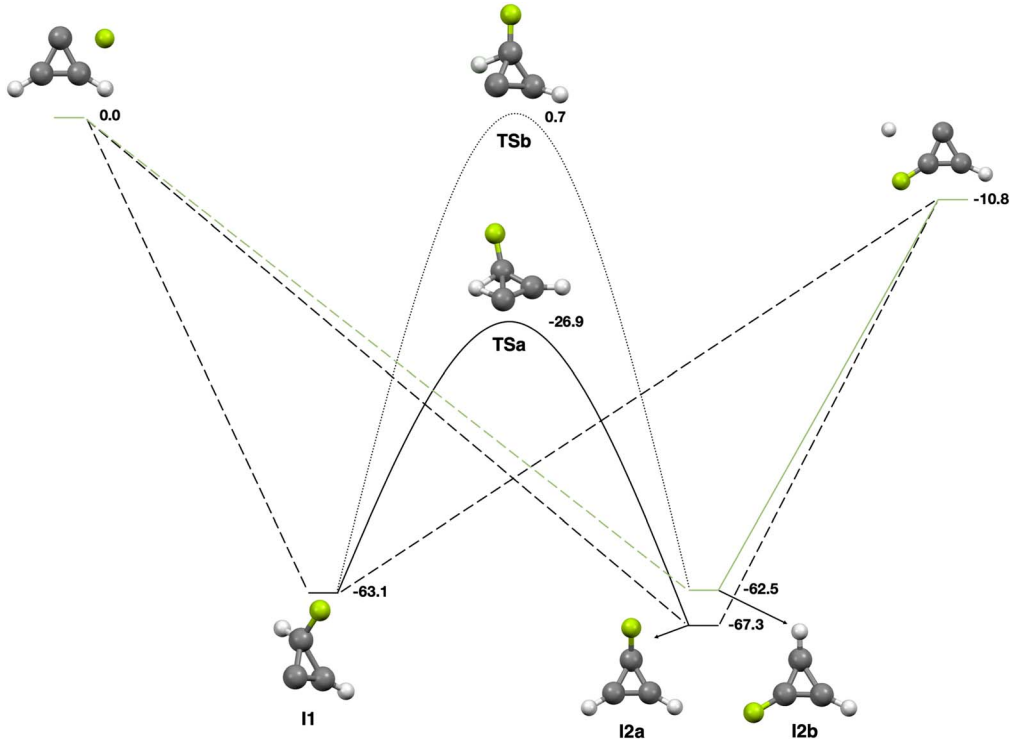

Figure 5. Reaction mechanism for the addition of ·F onto c-C_3H_2. Highlighted connections indicate the most energetically likely formation route.

3.3. Formation of c-C_3HF

The reaction pathway for the addition of ·F to c-C_3H_2 to form c-C_3HF is mapped in Figure 5. Like the addition of ·OH to c-C_3H_2, this reaction can proceed through an intermediate for which an analogous structure does not exist in the formation mechanism of c-C_3HC_2H. Unlike the ·OH pathway, this intermediate I2b is higher in energy than its conformer I2a. Intermediate I2b is also the highest-energy intermediate on the pathway as a whole. This reflects the increase in stabilization, comparatively, for the fluoro-substituted I2a as shown in Figure 4. The lowest occupied molecular orbital (LUMO) of this intermediate experiences greater orbital overlap between the electrons of the fluorine substituent and the p orbital of the carbon to which it is bound. Additionally, the orbital overlap in the SOMO-1 is far more significant in the fluoro intermediate. Upon examining the frontier MOs of I2b for these pathways (Figure 6), no significant differences are seen between the MOs for this type of intermediate upon swapping the substituent. The changes in energy, then, are mostly caused by increased stabilization in intermediates that are not I2b.

The higher energy of I2b for c-C_3HF formation relative to the other intermediates present on this pathway (-62.52 kcal mol^{-1} versus -63.13 kcal mol^{-1} (I1) and 67.31 kcal mol^{-1} (I2a)) results in a dissociation of a hydrogen atom from I2b with the smallest exit energy (51.74 kcal mol^{-1}) for product formation on this potential surface. This dissociation is facile, just as for the analogous intermediate on the ·OH addition pathway, and the dissociation of this complex does not require excitation into any higher electronic states. Association of ·F onto c-C_3H_2 to form this intermediate is barrierless.

The fluoro and hydroxyl addition pathways are strikingly similar, barring the additional structural complexity on the ·OH pathway due to rotation of the hydroxyl hydrogen. This is evidenced by the structures and energies of local optima, as well as the unique intermediate and dissociation pathway detailed in the previous paragraph. Therefore, both pathways

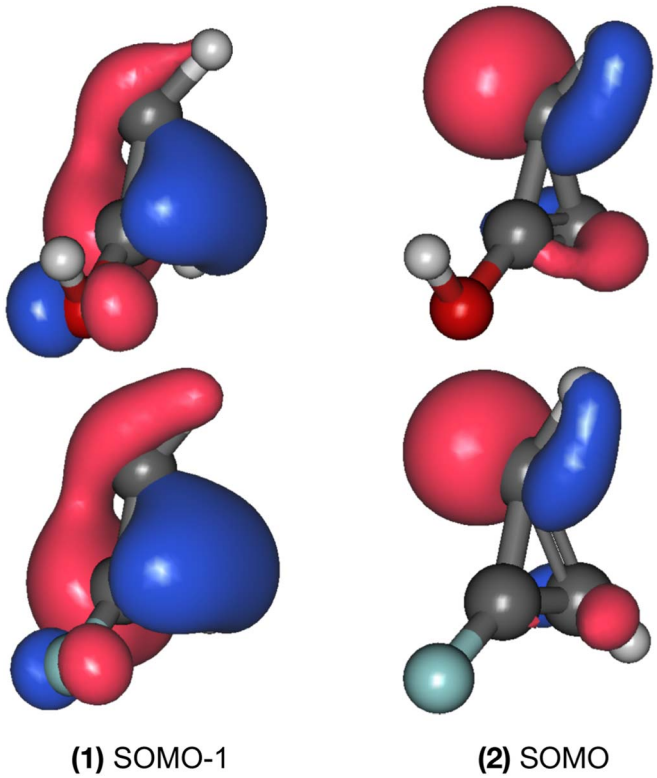

Figure 6. Frontier MOs of intermediate I2b for the formation of c-C_3HOH and c-C_3HF. For brevity, the lower-energy intermediate is taken for the c-$C_3H_2(OH)$ structure.

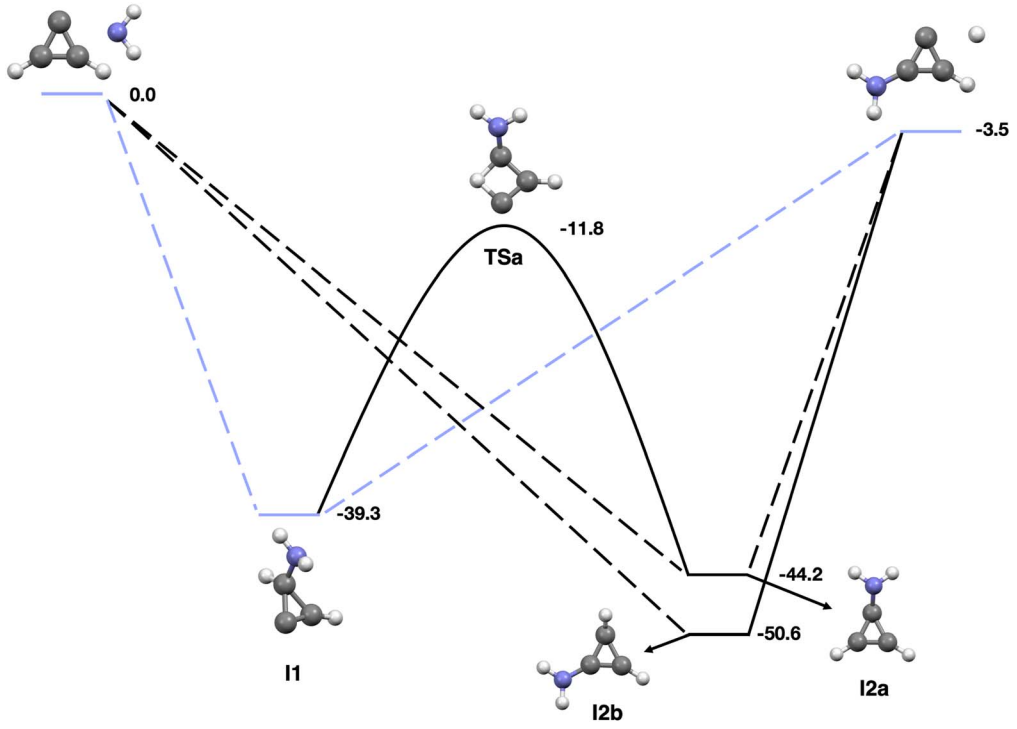

Figure 7. Reaction mechanism for the addition of $\cdot NH_2$ onto c-C_3H_2. Highlighted connections indicate the most energetically likely formation route.

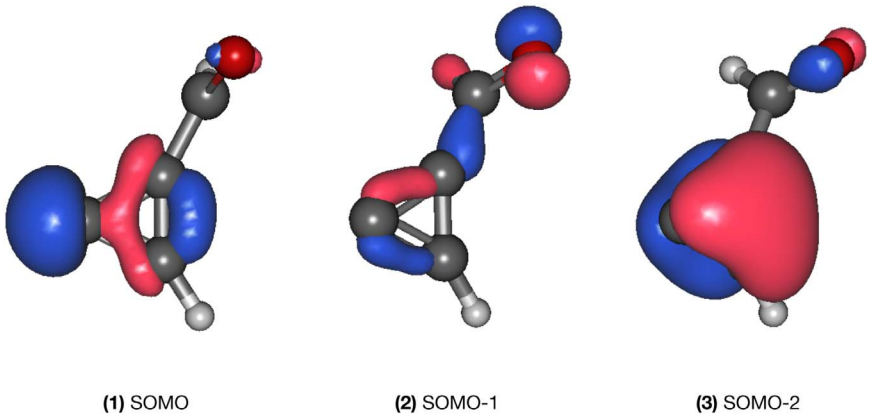

Figure 8. The three highest-occupied MOs of c-C_3HCHO.

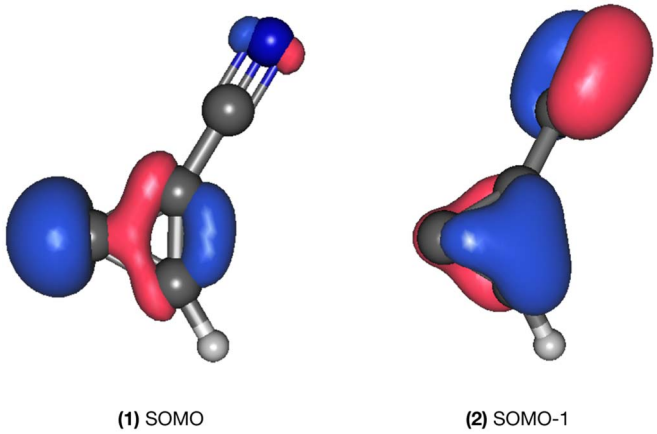

Figure 9. The two highest-occupied MOs of c-C_3HCN.

are likely to behave similarly on the whole with a similar number of opportunities for product formation when considering only the mechanism in isolation.

The significant energetic stabilization (-10.77 kcal mol^{-1}) upon addition of $\cdot F$ to c-C_3H_2, as well as the large dipole moment of c-C_3HF, shows promise for the formation and spectroscopic detectability of c-C_3HF. However, the small interstellar abundances of fluorine, even with atomic (Suess & Urey 1956; Cameron 1973; Jr & York 1981) and small molecule presence (Neufeld et al. 1997), make the probability of collision between the necessary species minimal. The circumstances surrounding the formation of fluorine in space (Woolsey & Haxton 1988; Woolsey & Weaver 1995; Meynet & Arnould 2000; Forestini et al. 1992) result in low concentrations of fluorine in the overall chemical budget of the universe. This association pathway, while energetically successful, serves more to guide current and future study of

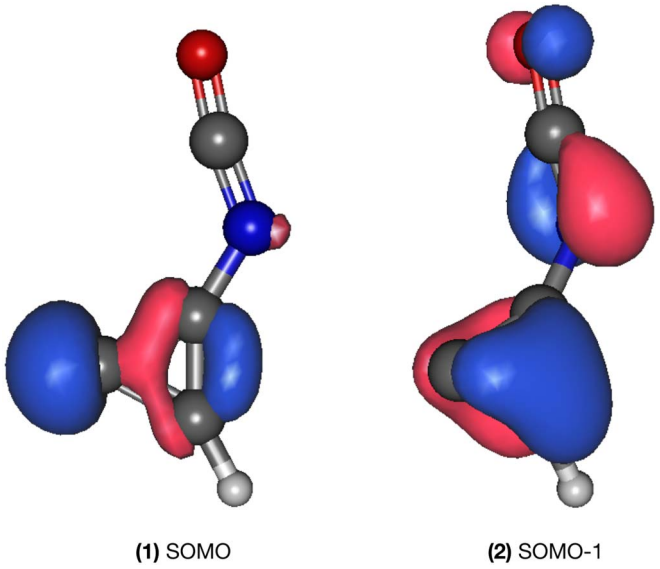

Figure 10. The three highest-occupied MOs of *c*-C_3HNCO.

neutral–radical reactivity in the ISM and laboratory studies of fluorine chemistry.

3.4. Formation of *c*-C_3HNH_2

The reaction pathway for the association of ·NH_2 onto *c*-C_3H_2 to form *c*-C_3HNH_2 is shown in Figure 7. Structures of local optima strongly resemble those seen in the ·OH and ·F addition pathways (Figures 3 and 5). Again, this pathway likely behaves in a very similar manner to that of the formation of *c*-C_3HOH in that one or more routes to product formation are barrierless. The presence of two hydrogens rather than one on the ring-bound substituent atom decreases the complexity of this pathway relative to that of *c*-C_3HOH. This pathway also has the most shallow submerged intermediates, with respect to the products, of any formation pathway presented here (see Table 3). These shallow wells incentivize product formation, potentially leading to high abundances of *c*-C_3HNH_2 if column densities of ·NH_2 allow for them.

3.5. Trends in Reactivity

The two most exothermic additions in Table 1 occur using triply bonded, linear radical species. The ability of the π electrons of the substituent to conjugate with the aromatic π system of *c*-C_3H_2 results in additional stabilization for the product of those additions. Two other additions—·CHO and ·NCO—also would allow electron delocalization in the product in theory, but the formation is not energetically favored. The structure of *c*-C_3HCHO, as given in Figure 1.6, shows that the formyl substituent lies nearly perpendicular to the plane of the cyclopropenylidene ring. This disallows significant interaction between the C−O π electrons and the *c*-C_3H_2 π system, as shown by the highest-energy occupied MOs in Figure 8. Successful additions, then, need the high degree of conjugation that additions of ·CN and ·C_2H provide, as provided by Figure 9. The failed addition of ·NCO is a different case. Figure 10 shows that the π orbitals of the substituent are indeed able to delocalize with the cyclopropenylidene ring as is necessary for product stabilization. However, examination of the SOMO and SOMO-1 of the ·NCO radical (Figure 11) shows that most of the electron density is not localized on the binding nitrogen atom. To access the orbital that displays this behavior, one must look back at the lower-energy SOMO-2. In contrast, the SOMO of the ·CN radical (Figure 12) shows a large amount of electron density on the binding carbon. Interactions between *c*-C_3H_2 and radicals with too little accessible electron density at the binding site are not strong enough to drive product formation. Figure 10 also shows a moderate fraction of the SOMO density located on the oxygen atom of ·NCO; however, a product formed with alternate connectivity (Figure 1.4) does not allow for π system extension and results in the least energetically favorable association of those calculated in Table 1. These outcomes create two criteria that must be simultaneously fulfilled in order for an association of this type to occur in the ISM.

The third through sixth entries in Table 1—the remaining exothermic additions—harbor unpaired electrons on second-row, highly electronegative atoms. The combination of lesser steric interactions between the incoming XH_n radical and *c*-C_3H_2 along with an increased ability to accept electron density from either site on *c*-C_3H_2 leads to successful additions for these three radical species. A general, periodic trend is created—as atomic size decreases and electronegativity increases, the energetic incentive for association becomes greater. The criteria set forth by Smith (2006), when applied to this chemical subspace, delineate that successful reactions of this class (as defined by a barrierless association between the two species) are constrained by the difference between the ionization energy of *c*-C_3H_2 and the electron affinity of the radical. Such reactions require a difference of 8.75 eV between these values to proceed barrierlessly. Since electronegativity and electron affinity roughly follow the same trend, reaction rates will increase along with exothermicity for this reaction class. This criterion also provides a guideline for further study of substituted cyclopropenylidenes: any radical with a greater electron affinity than that of the reactions shown to be barrierless here can also add barrierlessly.

It should also be noted that the addition of ·SiH_3 disrupts the observed trend discussed above. Where one would expect the addition of this radical to be more endothermic than that of ·PH_2 by the calculated energies, it is less endothermic by over 15 kcal mol^{-1}. The reason for this effect remains unknown, but the unusual energetic behavior of the silyl radical has been seen in other contexts, such as hydrogen abstractions (Burke et al. 2021).

4. Conclusion

Five substituted cyclopropenylidenes (*c*-C_3HCN, *ap*-*c*-C_3HOH, *sp*-*c*-C_3HOH, *c*-C_3HF, and *c*-C_3HNH_2) are shown to form through barrierless additions between *c*-C_3H_2 and the corresponding radical. All associations result in the formation of one or more submerged intermediates that release a hydrogen radical in the final step of the mechanism, producing the substituted cyclopropenylidene. With the exception of ·F, all radicals required to form these products are readily accessible in the ISM, which increases the probability of the detection of these species in interstellar space. The comparative reduction in the dipole moments and reaction energies of *c*-C_3HCN, *c*-C_3HF, and *ap*-*c*-C_3HOH to those of *c*-C_3HC_2H, the only currently confirmed *c*-C_3H_2 derivative, may hinder their detectability. However, their dipole moments of 3.06 D,

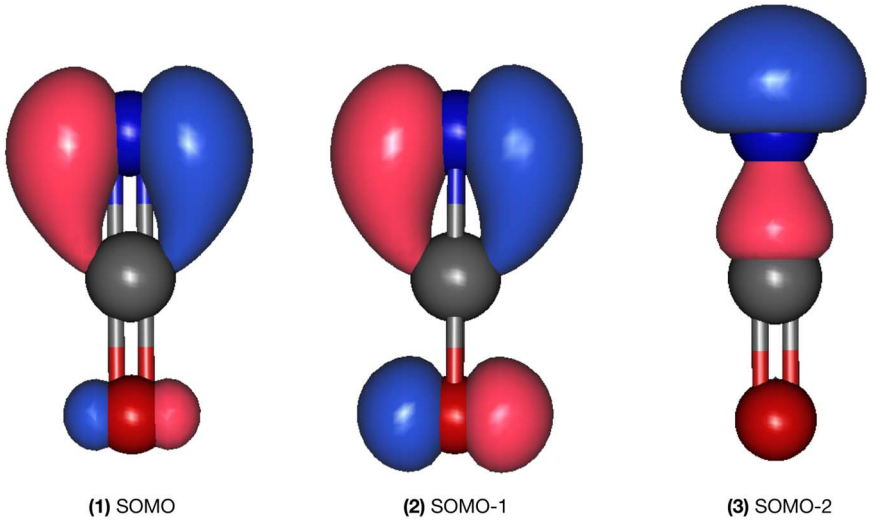

Figure 11. The three highest-occupied MOs of ·NCO.

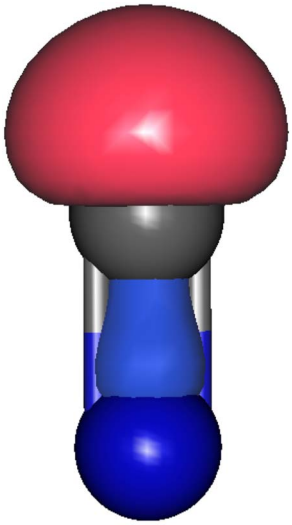

Figure 12. The SOMO of ·CN.

2.99 D, and 2.36 D, respectively, should still be plenty large enough to allow detection through rotational spectroscopy.

Both the five exothermic and 12 endothermic c-C_3H_2 substitutions presented in this work provide insight into the chemistry of the ubiquitous cyclopropenylidene molecule. Radical species that interact with c-C_3H_2 in the ISM appear to require a high electrophilicity and an ability to conjugate electron density with c-C_3H_2 in order to chemically react. The present results provide guidelines for the derivatives of c-C_3H_2 that may be present in the ISM. The reactivity of one of the smallest aromatic species in interstellar space may be linked to the chemistry of larger aromatic systems, such as benzene and polycyclic aromatic hydrocarbons.

The computing facilities required for this work are provided by the Mississippi Center for Supercomputing Research partially funded by NSF grant OIA-1757220. This work is supported by the University of Mississippi's College of Liberal Arts and NASA grant NNH22ZHA004C.

Software: Gabedit (Allouche 2017), GAUSSIAN16 (Frisch et al. 2019), MOLPRO2020.1 (Werner et al. 2020b), PSI4 (Turney et al. 2012; Parrish et al. 2017).

ORCID iDs

Athena R. Flint https://orcid.org/0000-0003-3881-0618
Ryan C. Fortenberry https://orcid.org/0000-0003-4716-8225

References

Adams, W. S. 1941, ApJ, 93, 11
Adler, T. B., Knizia, G., & Werner, H. 2007, JChPh, 127, 221106
Allouche, A.-R. 2010, JCoCh, 32, 174
Allouche, A. 2017, Gabedit, http://gabedit.sourceforge.net/
Amos, R. D., Andrews, J. S., Hardy, N. C., & Knowles, P. J. 1991, CPL, 185, 256
Bell, M. B., Feldman, P. A., Matthews, H. E., & Avery, L. W. 1986, ApJ, 311, L89
Brown, R. D., Godfrey, P. D., & Bettens, R. P. A. 1987, MNRAS, 227, 19
Burke, A. D., Bowman, M. C., Turney, J. M., & Henry, F. S. I. 2021, PCCP, 23, 3389
Cameron, A. G. W. 1973, SSRv, 15, 121
Cernicharo, J., Agúndez, M., Cabezas, C., et al. 2021, A&A, 649, L15
Chipman, D. M., & Miller, K. E. 1984, JAChS, 106, 6236
Cooper, D. L., & Murphy, S. C. 1988, ApJ, 333, 482
Cox, P., Guesten, R., & Henkel, C. 1987, A&A, 181, L19
Crutcher, R. M., Troland, T. H., & Heiles, C. 1981, ApJ, 249, 137
Deegan, M. J. O., & Knowles, P. J. 1994, CPL, 227, 321
Dickey, J. M., Crovisier, J., & Kazes, I. 1981, A&A, 98, 271
Domcke, W., & Yarkony, D. R. 2012, ARPC, 63, 325
Dunning, T. H. 1989, JChPh, 90, 1007
Forestini, M., Goriely, S., Jorissen, A., & Arnould, M. 1992, A&A, 261, 157
Fortenberry, R. C. 2021, ApJ, 921, 132
Frisch, M. J., Trucks, G. W., Schlegel, H. B., et al. 2019, Gaussian 16 Revision C.01 (Wallingford CT: Gaussian Inc.)
Gomez Gonzalez, J., Guelin, M., Cernicharo, J., Kahane, C., & Bogey, M. 1986, A&A, 168, L11
Grosselin, D., & Fortenberry, R. C. 2022, ESC, 6, 18
Győrffy, W., & Werner, H. 2018, JChPh, 148, 114104
Hampel, C., Peterson, K. A., & Werner, H. 1992, CPL, 190, 1
He, C., Fujioka, K., Nikolayev, A. A., et al. 2022, PCCP, 24, 578
Heikkilä, A., Johansson, L. E. B., & Olofsson, H. 1999, A&A, 344, 817
Heiles, C. E. 1968, ApJ, 151, 919
Henkel, C., Mauersberger, R., & Schilke, P. 1988, A&A, 201, L23
Herbst, E. 2001, Chem. Soc. Rev., 30, 168
Herbst, E. 2021, FrASS, 8, 776942
Hill, J. G., & Peterson, K. A. 2010, PCCP, 12, 10460
Hoffmann, M. R., Laidig, W. D., Kim, K. S., Fox, D. J., & Schaefer, H. F. 1984, JChPh, 80, 338

Jefferts, K. B., Penzias, A. A., & Wilson, R. W. 1970, ApJ, 61, L87
Jr, T. P. S., & York, D. G. 1981, ApJ, 247, L39
Kaiser, R. I. 2002, ChRv, 102, 1309
Karton, A., & Thimmakondu, V. S. 2022, JPCA, 126, 2561
Kendall, R. A., Dunning, T. H., & Harrison, R. J. 1992, JChPh, 96, 6796
Knizia, G., Adler, T. B., & Werner, H. 2009, JChPh, 130, 054104
Knowles, P. J., Andrews, J. S., Amos, R. D., Handy, N. J., & Pople, J. A. 1991, CPL, 186, 130
Knowles, P. J., Hampel, C., & Werner, H. 1993, JChPh, 99, 5219
Krylov, A. I. 2008, ARPC, 59, 433
Lee, T. J., & Taylor, P. R. 1989, IJQC, 36, 199
Lucas, R., & Liszt, H. S. 2000, A&A, 358, 1069
Madden, S. C., Irvine, W. M., & Matthews, H. E. 1986, ApJ, 311, L27
Madden, S. C., Irvine, W. M., Swade, D. A., Matthews, H. E., & Friberg, P. 1989, AJ, 97, 1403
Majumdar, L., Gratier, P., Andron, I., Wakelam, V., & Caux, E. 2017, MNRAS, 467, 3525
Matthews, H. E., & Irvine, W. M. 1985, ApJ, 298, L61
McCarthy, M. C., Grabow, J.-U., Travers, M. J., et al. 1999, ApJ, 513, 305
McGuire, B. A. 2021, ApJS, 259, 30
McKellar, A. 1940, PASP, 52, 187
Melosso, M., Bizzocchi, L., Sipilä, O., et al. 2020, A&A, 641, A153
Meynet, G., & Arnould, M. 2000, A&A, 355, 176
Møller, C., & Plesset, M. S. 1934, PhRv, 46, 618
Neufeld, D. A., Zmuidzinas, J., Schilke, P., & Phillips, T. G. 1997, ApJ, 488, L141
Nixon, C. A., Thelen, A. E., Cordiner, M. A., et al. 2020, AJ, 160, 205
Oike, T., Kawaguchi, K., Takano, S., & Nakai, N. 2004, PASJ, 56, 431
Parrish, R. M., Burns, L. A., Smith, D. G. A., et al. 2017, J. Chem. Theory Comput., 13, 3185
Peterson, K. A., Adler, T. B., & Werner, H. 2008, JChPh, 128, 084102
Puzzarini, C. 2022, FrASS, 8, 811342
Qi, C., Öberg, K. I., Wilner, D. J., & Rosenfeld, K. A. 2013, ApJ, 765, L14
Raghavachari, K., Trucks, G. W., Pople, J. A., & Head Gordon, M. 1989, CPL, 157, 479
Ramal-Olmedo, J. C., Menor-Salván, C. A., & Fortenberry, R. C. 2021, A&A, 656, A148
Schuurman, M. S., & Stolow, A. 2018, ARPC, 69, 427
Seaquist, E. R., & Bell, M. B. 1986, ApJ, 303, L67
Seburg, R. A., McMahon, R. J., Stanton, J. F., & Gauss, J. 1997, JAChS, 119, 10838
Smith, I. W. M. 2006, AngCh, 45, 2842
Smith, I. W. M. 2011, ARA&A, 49, 29
Spezzano, S., Brünken, S., Schille, P., et al. 2013, ApJ, 769, L19
Spezzano, S., Tamassia, F., Thorwirth, S., et al. 2012, ApJS, 200, 1
Stanton, J. F., & Bartlett, R. J. 1993, JChPh, 98, 7029
Storey, J. W. V., Watson, D. M., & Townes, C. H. 1981, ApJ, 244, L27
Suess, H. E., & Urey, H. C. 1956, RvMP, 28, 53
Tan, X., Wang, W., Jing, Y., Wang, F., & Li, P. 2014, Monatsh. Chem., 145, 1109
Teyssier, D., Fossé, D., Gerin, M., et al. 2004, A&A, 417, 135
Thaddeus, P., Guelin, M., & Linke, R. A. 1981, ApJ, 246, L41
Thaddeus, P., Vrtilek, J. M., & Gottlieb, C. A. 1985, ApJ, 299, L63
Travers, M. J., McCarthy, M. C., Gottlieb, C. A., & Thaddeus, P. 1997, ApJ, 483, L135
Turney, J. M., Simmonett, A. C., Parrish, R. M., et al. 2012, WIREs Comput. Mol. Sci., 2, 556
van Dishoeck, E. F., Jansen, D. J., Schilke, P., & Phillips, T. G. 1993, ApJL, 416, L83
Vrtilek, J. M., Gottlieb, C. A., & Thaddeus, P. 1987, ApJ, 314, 716
Weinreb, S., Barrett, A. H., Meeks, M. L., & Henry, J. C. 1963, Nat, 200, 829
Werner, H., Knowles, P. J., Knizia, G., Manby, F. R., & Schütz, M. 2012, WIREs Comput. Mol. Sci., 2, 242
Werner, H., Knowles, P. J., Manby, F. R., et al. 2020a, JChPh, 152, 144107
Werner, H., Knowles, P. J., Knizia, G., et al. 2020b, MOLPRO, v2020.1, a package of ab initio programs, https://www.molpro.net
Westbrook, B. R., Patel, D. J., Dallas, J. D., et al. 2021, JPCA, 125, 8860
Woolsey, S. E., & Haxton, W. C. 1988, Nat, 334, 45
Woolsey, S. E., & Weaver, T. A. 1995, ApJS, 101, 181
Woon, D. E., & Dunning, T. H. 1993, JChPh, 98, 1358
Yang, Z., Doddipatla, S., Kaiser, R. I., et al. 2021, ApJL, 908, L40
Yarkony, D. R. 2001, JPCA, 105, 6277